Microsyst Technol (2009) 15:1547–1556
DOI 10.1007/s00542-009-0803-8

TECHNICAL PAPER

Design and construction of an in situ inspection machine for ensuring the dynamic performance of fluid bearings in data storage devices

Paul C.-P. Chao · Chi-Wei Chiu · J.-S. Huang · Chien-Ming Chen

Received: 31 July 2007 / Accepted: 30 January 2009 / Published online: 21 February 2009

Abstract The objective of the study is to design and construct an in situ inspection machine that would be used to evaluate the dynamic performance of the small-scaled hydrodynamic journal bearings used often for data-storage devices. To this end, novel design ideas of using a high-stiffness air bearing and suspending the test bearing by the specially-designed fixture frame are first proposed, which are accompanied by the special requirements in the manufacturing precisions for various dimensions and geometry characteristics of the components of the experiment system. The capacitor-type sensors, including two custom-mades are next utilized to measure the motions of the spindle and bearing. Finally, a calculating algorithm for deriving performance parameters of the test bearing are proposed, which is intended primarily to estimate rotor stiffness coefficients, load capacity, and eccentricity ratio to determine if the test bearing meet the dynamic performance expected by the original design.

1 Introduction

The data storage capacity of hard disk drives is increased in an amazing speed as a result of several key technology advancements in recording data on a disk with very high areal density. Recently, the areal density of hard disk drives has been increasing at a growth rate of 100%. The early-day limit of areal density of 40 GB/in has been broken. It is expected that the areal density will soon reach the level of 100 GB/in Therefore it is anticipated that the allowable nonrepeatable run out (NRRO) of spindle motors has to be suppressed to below 1 μm, which is required in high track density recording. In additions, the hard disk drives need also to work faster, quieter and more reliable. All of these mentioned performances necessitate further improvements for the spindle motor.

It is known that the performance of a spindle motor largely depends on the performance of its bearings. Therefore, the bearing system becomes a key technology for the advancement of the spindle motor. In recent years, the fluid-film bearing or namely hydrodynamic journal bearings (HJB) becomes the popular choice for the high-speed spindle motors owing to its dynamic characteristics of lower non-repeatable runouts, lower acoustic noise, higher stiffness and higher damping coefficients, as compared to conventional ball bearings (Zhang et al. 1999). To estimate the dynamic coefficients, several methods were proposed in the past study, such as selective vibration orbits (Brockwell and Dmochowski 1989) etc. The method, however, estimates the coefficients by collecting the data in the discrete time, which may lead to the error in the measurements under the high speed operation. To meet this demand of fast and precise developments in varied types of HJB, an in situ and in-lab inspection machine for evaluating the dynamic performance of fluid bearings in data storage devices, including hard and optical disk drives, is successfully designed and constructed in this study.

To determine the rotordynamic coefficients of an HJB, an appropriate data analysis method must be selected based on the experimental setup and excitation type used.

P. C.-P. Chao (✉) · C.-W. Chiu
Department of Electrical and Control Engineering,
National Chiao Tung University, Hsinchu 300, Taiwan
e-mail: pchao@mail.nctu.edu.tw

J.-S. Huang · C.-M. Chen
Department of Mechanical Engineering, R&D Center
for Membrane Technology, Chung-Yuan Christian University,
Chung-Li 320, Taiwan

Identification methods can be divided into two general categories: time domain methods and frequency domain methods. One example of a time domain used for bearing parameter identification is the Kalman Filter (Fritzen and Seibold 1990; Mohanmmad and Burdess 1990). Even though time domain methods do not require transformation of the data to the frequency domain, they are generally nonlinear problems, which must be solved by iterative processes. The analysis used by Brockwell and Dmochowski (1989), for straight line orbit excitation, may also be classified as a time domain method. The coefficients are determined from measurements at discrete times when only one velocity or displacement is non-zero. This method tends to results in large errors, since only selected points are used to exact the coefficients, instead of the entire time histories. Furthermore, inertia coefficients cannot be found by this method. On the other hand, frequency domain methods are well suited for the analysis of data obtained from multiple-frequency excitation methods. For linear systems, the multi-frequency excitation and response data are expressed in the frequency domain as a series of discrete frequency responses. The rotordynamic coefficients can be extracted directly from frequency domain data by rewriting the equations in such a way that the coefficients appear in a vector, and then using a least squares formulation to estimate the coefficient values (Burrows et al. 1987; Nordmann and Massmann 1984). This method gives more insight into the bearing characteristics, and provides valuable information in analyzed data. In addition to the general frequency method, the excitation input wave form has to be determined to calculated low-noised coefficients. The main criteria in selecting an excitation waveform should be to achieve a response sufficiently higher than the noise, but small enough that it does not violate the linearity assumption. With multiple frequency excitation methods, satisfactory signal to noise (S/N) ratios are difficult to achieve without averaging. For deterministic signals, time domain averaging is used (Nordmann and Massmann 1984) (or equivalently averaging of the Fourier transforms), while for random signals, power spectral densities must be used (Yasuda et al. 1986). However, Rouvas et al. (1992) have shown that power spectral density methods can be used to averaging deterministic signals. Power spectral density methods are shown to eliminate errors caused by variations in the deterministic excitation signals used for averaging some amount of variation if vibration being inadvertently present in any measured signal. Following the aforementioned idea if identification, Childs and Hale (1994) synthesize an identification scheme to derive low-noised estimation of rotordynamic coefficients of a testing rig for HJBs. This scheme is followed by the current study to design/build an in situ bearing inspection machine for performing coefficient estimation.

The proposed inspection machine consists mainly of a driving motor, a flexible coupling, an air bearing, positioning fixtures, a newly-designed suspension for the test bearing, a shaker to exert exciting forces on the test bearing and two capacitor-type sensors. The key, the novel idea of the inspection machine design lies in the use of the high-stiffness air bearing to maintain radial run-outs of the spindle below 1 μm, and the suspension in a specially-designed fixture structure to allow the test bearing case in relatively-free motions to the spindle with much higher stiffness induced by the lubrication oil of the bearing. The air bearing for the inspection machine are selected to the special requirements in the manufacturing precisions for various dimensions and geometry characteristics of the components of the inspection machine. The capacitor-type sensors, including two custom-made ones, are also utilized to measure the motions of the spindle and bearing. Applying prespecified external force on the test fluid bearing by the shaker in desired frequency contents and acquiring relative radial motion between the test bearing case and the spindle based on the measurements from capacitor-type sensors, the dynamic coefficients of the test fluid-film bearing can then be calculated by the algorithm forged for deriving performance parameters of the test bearing. The algorithm is designed primarily to estimate rotor stiffness coefficients, load capacity, and eccentricity ratio to determine if the test bearing meet expected dynamic performance. In this algorithm, the rotordynamic coefficients are extracted directly from frequency domain data by rewriting the equations in a way that the coefficients appear in a vector, and using a least squares formulation to estimate the coefficient values (Burrows; Nordmann). Finally, the experimentally-estimated dynamic coefficients of the bearing are compared to theoretical estimates (Kawabata et al. 1989; Chao and Haung 2005), demonstrating favorable performance of the inspection machine.

This paper is organized as follows. Section 2 states the design ideas and detailed description on the experiment system. Section 3 derives the dynamics model of the experiment system, along with methods of identification. Section 4 gives results and discussion. Section 5 concludes this study and present future works.

2 The inspection machine

The design idea and detailed description on the in situ inspection machine are provided in this section for the further employment of the experimental identification algorithm presented in the next section to estimate the dynamic coefficients of the bearings.

2.1 Theoretical basis for experiment

The configuration of the in situ inspection machine is depicted in Fig. 1a, while Fig. 1b presents a picture of the realistic in situ inspection machine in a entire experimental setup for testing the performance of a hydrodynamic journal bearing (HJB). It is seen from Fig. 1a or b that the designed in situ inspection machine consists of three parts: (1) a motor frame to support the driving motor; (2) an high-stiffness air bearing to offers relative stillness of the test bearing; (3) a suspension frame to support the test bearing. Between the motor frame and the air bearing is a flexible coupling to isolate the vibration of the driving motor to the rest of the inspection machine. Theoretical basis for identification originates from Child and Hale (1994). In identification, the external excitation forces and measurements are applied and recorded, respectively, at the test HJB and spindle. The measurements will be used to explore HJB performance. Focusing on the subsystem of bearing, suspension, and spindle, the third part of Figs. 1a and 2 illustrates the theoretical basis of the experiment identification. Figure 2 in fact displays free body diagrams of two rigid bodies—the spindle and the HJB for testing. In this figure, $\{f_x, f_y\}$ are x and y components of the input excitation

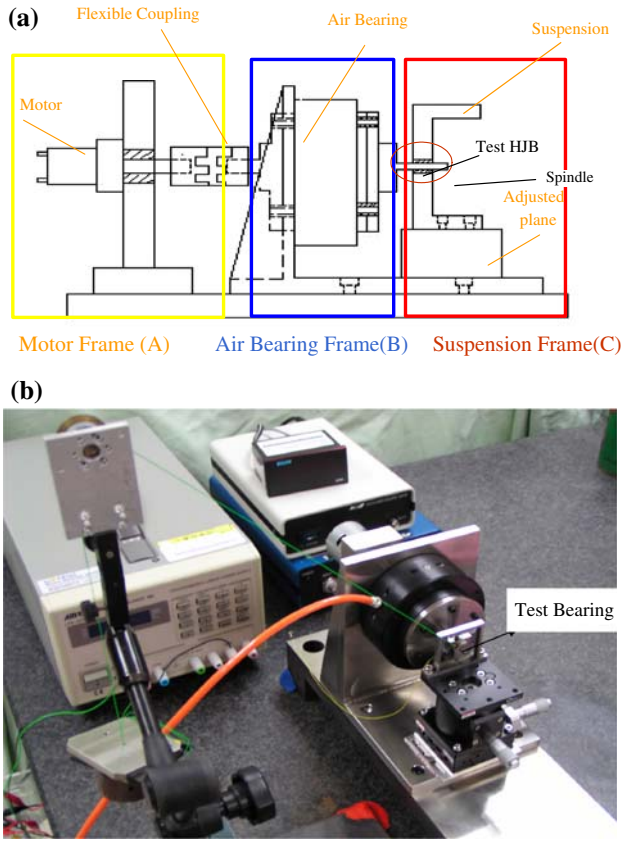

Fig. 1 (**a**) The experimental diagram. (**b**) The experimental setup including the in situ inspection machine

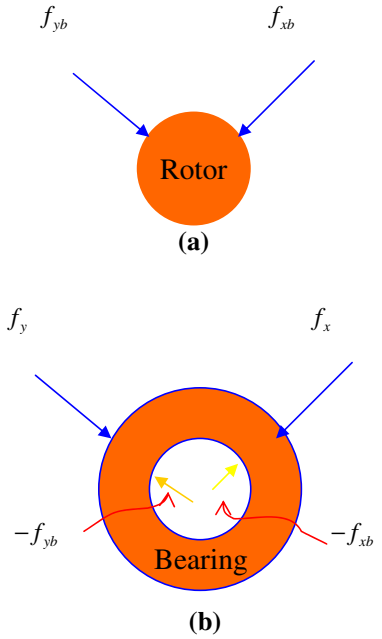

Fig. 2 The theoretical basis of the experiment

forces exerted by shaker. As the test bearing in vibration, there are bearing reaction forces, denoted by $\{f_{xb}, f_{yb}\}$, acting on the spindle as shown in Fig. 2a, while becoming $\{-f_{xb}, f_{yb}\}$ at the bearing inner surface in Fig. 2b. Based on the free body diagram in Fig. 2, the equations of motion for the stator (bearing) mass M_s in Fig. 2 can be written by

$$M_s \begin{Bmatrix} \ddot{x}_s \\ \ddot{y}_s \end{Bmatrix} = \begin{Bmatrix} f_x \\ f_y \end{Bmatrix} + \begin{Bmatrix} f_{xb} \\ f_{yb} \end{Bmatrix}, \tag{1}$$

where $\{\ddot{x}_s, \ddot{y}_s\}$ the (measured) components of the stator's acceleration, bearing reaction forces $\{f_{xb}, f_{yb}\}$ are, based on simple dynamics,

$$-\begin{Bmatrix} f_{bx} \\ f_{by} \end{Bmatrix} = \begin{bmatrix} K_{xx} & K_{xy} \\ K_{yx} & K_{yy} \end{bmatrix} \begin{Bmatrix} \Delta x \\ \Delta y \end{Bmatrix} + \begin{bmatrix} C_{xx} & C_{xy} \\ C_{yx} & C_{yy} \end{bmatrix} \begin{Bmatrix} \Delta \dot{x} \\ \Delta \dot{y} \end{Bmatrix} + \begin{bmatrix} M_{xx} & M_{xy} \\ M_{yx} & M_{yy} \end{bmatrix} \begin{Bmatrix} \Delta \ddot{x} \\ \Delta \ddot{y} \end{Bmatrix}, \tag{2}$$

Combining Eqs. (1) and (2) gives

$$\begin{Bmatrix} f_x - M_s \ddot{x}_s \\ f_y - M_s \ddot{y}_s \end{Bmatrix} = \begin{bmatrix} K_{xx} & K_{xy} \\ K_{yx} & K_{yy} \end{bmatrix} \begin{Bmatrix} \Delta x \\ \Delta y \end{Bmatrix} + \begin{bmatrix} C_{xx} & C_{xy} \\ C_{yx} & C_{yy} \end{bmatrix} \begin{Bmatrix} \Delta \dot{x} \\ \Delta \dot{y} \end{Bmatrix} + \begin{bmatrix} M_{xx} & M_{xy} \\ M_{yx} & M_{yy} \end{bmatrix} \begin{Bmatrix} \Delta \ddot{x} \\ \Delta \ddot{y} \end{Bmatrix}, \tag{3}$$

where

$$\Delta x(t) = x - x_s \text{ and } \Delta y(t) = y - y_s. \tag{4}$$

with known M_s and $\{x, y, x_s, y_s\}$, the motions of spindle and bearing, measurable from sensors, the dynamic

coefficients M's, C's, and K's can be identified based on Eq. (3) via a calculating algorithm to be developed in the next section.

In order to obtain satisfactory identification results, the generation of $\Delta x(t)$ and $\Delta y(t)$ via Eq. (4) into Eq. (3) ought to render large sensor-to-noise (S/N) ratio, which leads to one of experiment design directives that the spindle is supported by a high-stiffness air bearing to contain the radial runouts of the spindle $\{x, y\}$ within small ranges, as compared to those radial vibrations of the bearing $\{x_s, y_s\}$, which are only constrained by the specially-designed suspension frame with relatively soft stiffness. From another point of view, on the contrary to the practical operation of a fluid-film bearing where the bearing is fixed while the spindle exerts radial vibration, in this experiment design the spindle is relatively motionless relatively to the bearing. Note also from Eq. (3) that beside the measurements of $\{x, y, x_s, y_s\}$, certain types of forces $\{f_x, f_y\}$ need to be applied at the bearing wall to generate nonzero measurements of $\{x, y, x_s, y_s\}$ for identifying rotordynamic coefficients. Thus, this generation of $\{f_x, f_y\}$ is part of experiment design. The general directives of determining $\{f_x, f_y\}$ are that $\{f_x, f_y\}$ have to be the dynamic loads with rich frequency content in almost-equal levels to each other of measurement in displacements, velocities and acceleration of $\{x, y, x_s, y_s\}$. In this way, as applying Eq. (3) for identifying M's, C's, and K's, the S/N ratios accompanied with estimated M's, C's, and K's, are commensurate. With the measurement of $\{x, y, x_s, y_s\}$ rich in frequency content, a calculating algorithm is developed in the next section to obtain satisfactory estimates of the rotordynamic coefficients.

Some further simplification steps are adopted to obtain preliminary estimates on rotordynamic coefficients. Considering the fact of thin fluid film for the bearing used for storage device and that no lubrication oil pumped in or out of the bearing during operation, the inertia effects on the dynamics of the system in Eq. (3) are small as compared to those of dampings and stiffness. Henceforth, the inertial terms in Eq. (3) is ignored in section four of experiment conduction. In addition, one can only applied static load other than dynamic ones to bearing wall, in which way all characteristics indices of the bearing except for the damping coefficients can be obtained. In the experiment conduction of this study, only the static load is applied to render preliminary estimation on bearing stiffness. Other than the application of the dynamic load is provided by shakers, the static load can be realized, as illustrated in Fig. 3 and photographed in Fig. 1b, by screwing a string at the bearing wall, stretching it through a pulley, and suspending with a designated weight. Note that the line of action of the static load (directed along the string and through the center of the bearing) is designed herein to have an angle of 45 degree relative to the horizontal, which makes easy the setup of the sensor system.

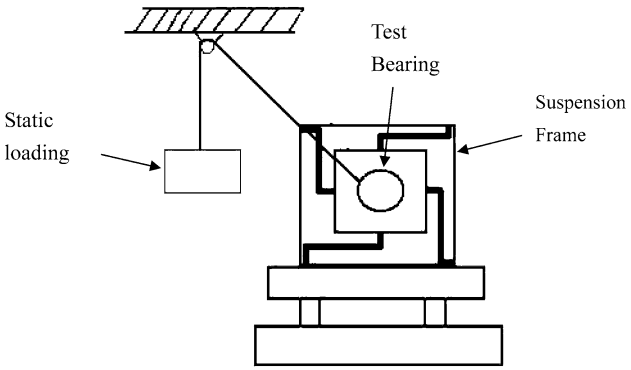

Fig. 3 Static loading system

2.2 Required specifications on components

2.2.1 Driving motor and fixture

A DC motor made by NICHIBO Corp. is utilized in this study, which can rotate the rotor above 18,000 rpm without loading. A supporting frame is designed and manufactured as shown in Fig. 4. Note that the vibrations induced by the DC motor are not particularly required to be small since

Fig. 4 The motor frame

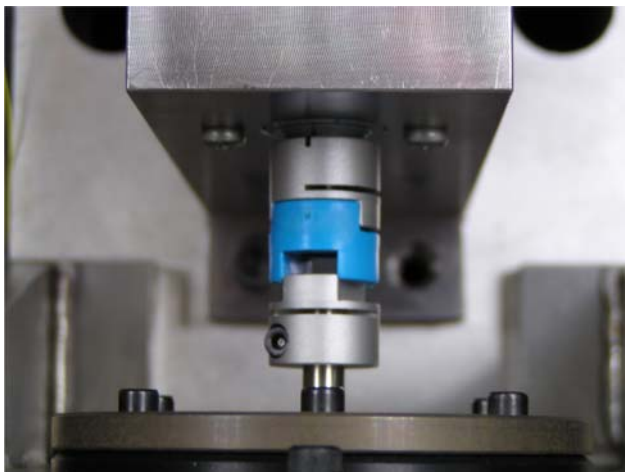

Fig. 5 The flexible coupling

they are expected to be damped out by the flexible coupling connected to spindle of the motor.

2.2.2 *Flexible coupling*

A flexible coupling in a particular geometric design is shown in Fig. 5. This function of this coupling is provide enough flexibility to damp put the vibrations induced by the power source, the motor, before the rotational spindle enters into the high-stiffness air bearing. Note that during experiment, the tightness in assembling two pieces of the coupling and interconnecting blue piece in Fig. 5 are adjusted through trials to render small spindle runouts at bearing location.

2.2.3 *Air bearing*

An air bearing made by, as shown in Fig. 6, is utilized in this study to exert high stiffness on the rotational spindle,

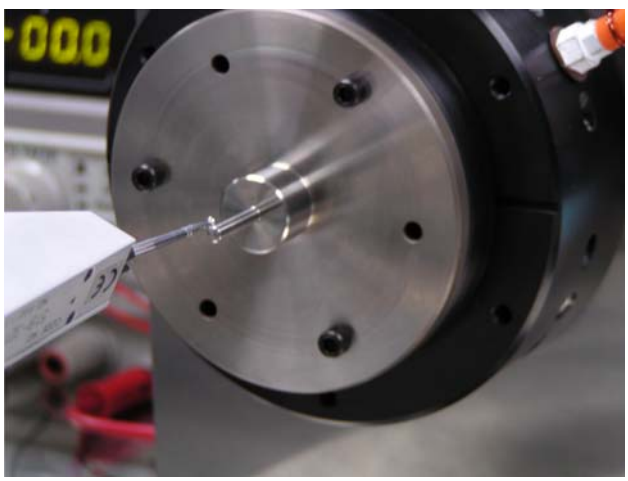

Fig. 6 The air bearing

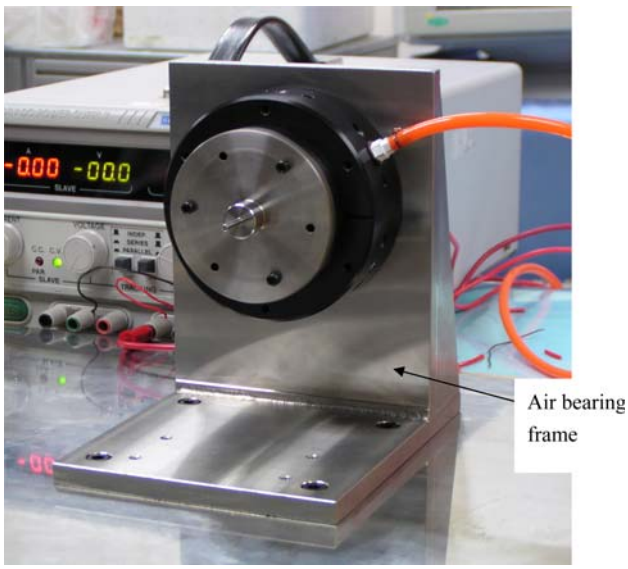

Fig. 7 The air bearing frame

resulting in a small spindle runouts around 1 μm at bearing location. The set of the air bearing consists of the bearing itself, a compressor providing air, and set of air purifiers to keep the inner compartment of the air bearing free of contamination. Other than a right choice of the air bearing, the supporting frame of the air bearing, as shown in Fig. 7, needs also to be designed stiff enough with natural frequencies above 1.0E + 6 N/um and manufactured in high precision to accomplish the goal of providing high stiffness. Note that he verticalness and flatness of the vertical contact planar surface of the frame to the air bearing are two critical manufacturing qualities required.

2.2.4 *The suspension frame*

The suspension frame supporting the test bearing is designed in particular geometry, as shown in Fig. 8a. This particular geometry would be able to provide much softer stiffness in radial direction as opposed to those in axial of the spindle. As results, the radial stiffness during experiment is mostly contributed from bearing stiffness. To ensure the stiffness of the suspension frame as desired, finite element analysis is conducted, as shown in Fig. 8b, to determine various dimensions of the suspension frame. It is shown from Fig. 8b that the radial stiffness of the suspension frames is 2.8 N/m which is much smaller than those of commercial bearings, which are within the ranges of 3.0E + 07 N/m. It is worthy to point out at this point that the design of the supporting frame also suits well for the needs of exchanging the bearings in various sizes for frequent tests.

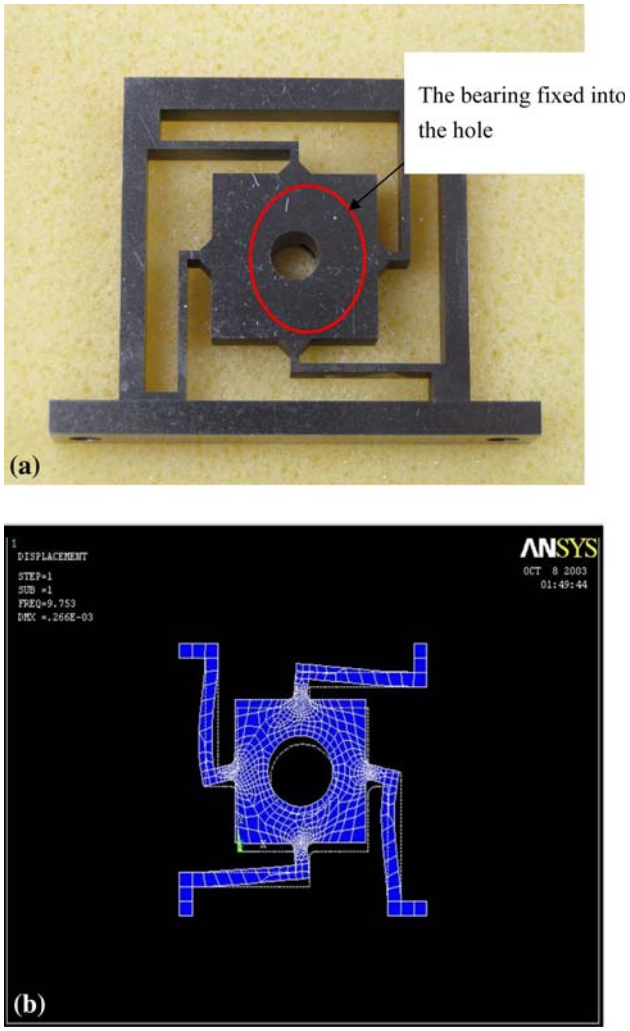

Fig. 8 (**a**) The suspension frame; (**b**) The finite element analysis

2.3 Sensing system

1. For spindle runouts, $\{x, y\}$: Two custom-made capacitor-type sensors as shown in Fig. 9a are used for measuring the runouts of the small-size spindle of 3 mm in diameter.
2. For bearing vibrations, $\{x_s, y_s\}$: Two common capacitor-type sensors as shown in Fig. 9b are used for measuring the vibrations of the bearing wall in X and Y directions.
3. For rotor speed, a common fiber-optic-type non-contact sensor is used to report the rotational speed of the rotor. The measuring range is from 10 to 99999 rpm.
4. The Cantilever-beam-type fixtures employed for the four capacitor-type sensors are required to be strong enough to sustain environmental vibrations. Pre-calibrations have been done to assists the selection of the fixtures in the purpose of ensuring the stiffnesses high enough to avoid extra commensurate vibration.

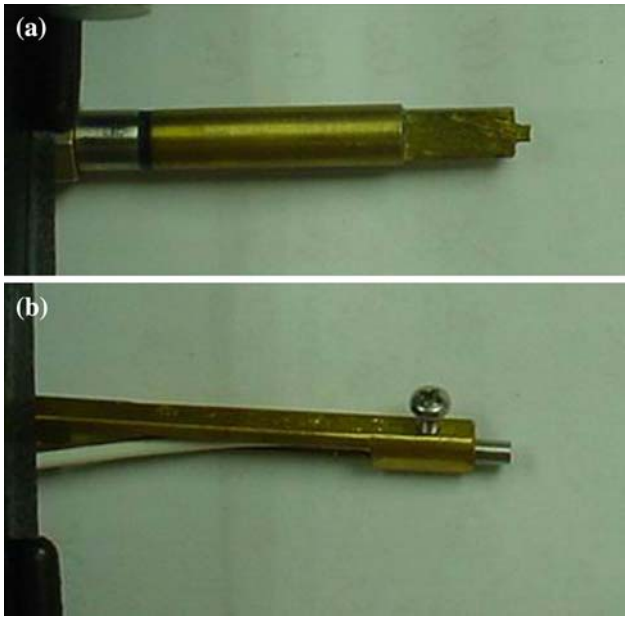

Fig. 9 (**a**) The custom-made capacitor-type sensors. (**b**) The common capacitor-type sensors

2.4 Experiment steps

The experiment steps for the case of applying static loads to identify various parameters of bearing performance from measurements are detailed in the followings.

1. Place the desired weight to the end of suspending string
2. Choose the test speeds as 2,000, 3,000, 4,000, 4,500 rpm, which, in experiments, are achieved by applying 1.32, 1.74, 2.2, 5.5 V to the DC motor, respectively.
3. Turn on the power supply and adjust the input volt to render the rotation speed steadily at the desired rpms, which is assured by the optic-fiber speed sensor.
4. Record measurement data in specified time period of 5 s from four capacitor-type sensors for spindle runouts and bearing vibration via an A/D card and data-acquisition software, while the rotation speed is steady on applied voltage. Within the 5 s, 5,000 data are taken from each of four capacitor-type sensors.
5. Take average of one oscillating period on data for first-level noise reduction.
6. Incorporate the averaged data into the algorithms developed for calculating various performance factors of the test bearing.

3 Identification of dynamic coefficients

The algorithm for calculating rotordynamic coefficient is developed herein, which is originated from Childs and Hale (1994).

3.1 Equations for identification

The rotordynamic coefficients are determined in the frequency domain via the Fourier Transform $\Im$ on Eq. (3), which yields

$$\begin{Bmatrix} F_x - M_s A_s \\ F_y - M_s A_s \end{Bmatrix} = \begin{bmatrix} H_{xx} & H_{xy} \\ H_{yx} & H_{yy} \end{bmatrix} \begin{Bmatrix} D_x \\ D_y \end{Bmatrix}, \tag{5}$$

where

$$F_k = \Im(f_k),\ A_k = \Im(\ddot{k}_k),\ D_k = \Im(\Delta k),$$

and k could be x or y. The elements of the frequency-response function (FRF) H are related to the coefficients defined in Eq. (3) by

$$H_{ij} = (K_{ij} - \omega^2 M_{ij}) + j(\omega C_{ij}), \tag{6}$$

where ω is the excitation frequency and $j = \sqrt{-1}$. It should be note that Eq. (5) only provides two complex equations for the four unknown H_{ij}'s. To successfully estimate all rotordynamic coefficients, two independent orthogonal dynamic loads are applied to the stator of the test bearing by alternately exciting along the X and Y directions in Fig. 2. Each of these "pseudo-random" dynamic loads contains 41 sinusoids. The superposition of these sinusoids is optimized to provide a composite loading that has a high $\Im$ spectral-line energy to high S/N ratio. The loadings are periodic and have energy only at 10 Hz frequency increments in the range from 100 to 500 Hz. The two independent loadings result in the four complex equations,

$$\begin{bmatrix} F_{xx} - M_s A_{xx} & F_{xy} - M_s A_{xy} \\ F_{yx} - M_s A_{yx} & F_{yy} - M_s A_{yy} \end{bmatrix} = \begin{bmatrix} H_{xx} & H_{xy} \\ H_{yx} & H_{yy} \end{bmatrix} \begin{bmatrix} D_{xx} & D_{xy} \\ D_{yx} & D_{yy} \end{bmatrix} \tag{7}$$

where the subscripts iy of the force and displacement matrices correspond to response in the i direction as shown in Fig. 2. Childs and Hale (1994) provides complete details of using the power-spectral density method by Bendat and Peirsol (1986) to calculate the H_{ij} functions. Spectral density averaging techniques are next used to obtain the frequency-response functions (FRF) of Eq. (7) for damping out noises, which defines a multi-input multi-output (MIMO) system. The details are stated in Appendix 1.

4 Results and discussion

Conducting the experiment steps as given in Sect. 2.4, one can obtain sensor outputs for the motions of the spindle and bearing, and their differences for later analysis. The varied parameters of the test HJB are listed in Table 1. Figure 10 show the measured motion difference between the spindle and bearing, i.e., $\Delta x(t) = x - x_s$ and $\Delta y(t) = y - y_s$, where the measurements in three spindle-rotating periods at the steady state are shown. It can be seen from these figures that the motions of the spindle and bearing should be both periodic and harmonic-like with low noises in one rotation of the spindle. Therefore, the results obtained from the computation procedure based on Eq. (7) are reliable to identify the rotordynamic coefficients of the test HJB.

With experimental data in hand by conducting those steps in Sect. 2.4, three related characteristics indices of the test bearing are calculated. They are load capacity, attitude angle, and two stifnesses coefficients. Figure 11 shows the load capacity with respect to various rotor speeds of 2,000, 3,000, 4,000, and 4,500 rpm, and also theoretical predictions obtained based on the model and computation procedure established in (Kawabata et al. 1989; Chao and Haung 2005) for rotor speed of 3,500 rpm. It is seen from this figure that the load capacity increases slowly as the eccentricity is low until the eccentricity reaches around 0.6. It reflects the fact that the bearing has higher capacity as the rotor exhibits higher eccentricity, which conforms to common performance of a bearing. On the other hand, the theoretical capacities for 3,500 rpm are in the vicinity of corresponding experimental data. In particular, the theoretical capacity at the eccentricity of 0.71 is between experimental counterparts of 3,000 and 4,000 rpms, showing the legitimacy of the in situ inspection machine built in this study. Figure 12 shows the attitude angle with respect to various rotor speeds, where the attitude angle keeps constant around within the range of low eccentricity and then moderately decreases approximately above the eccentricity of 0.7. The change in the

Table 1 The bearing specifications

Bearing diameter	6 mm
L/D ratio	1.5
Radial clearance	2 μm
Bearing mass	10.577 g
Groove depth	5 μm
Groove angle	21°
Groove values	8
Fluid viscosity	0.0297 N s/m^2
Operating speed	2,000–4,500 rpm
Static load	35–350 g

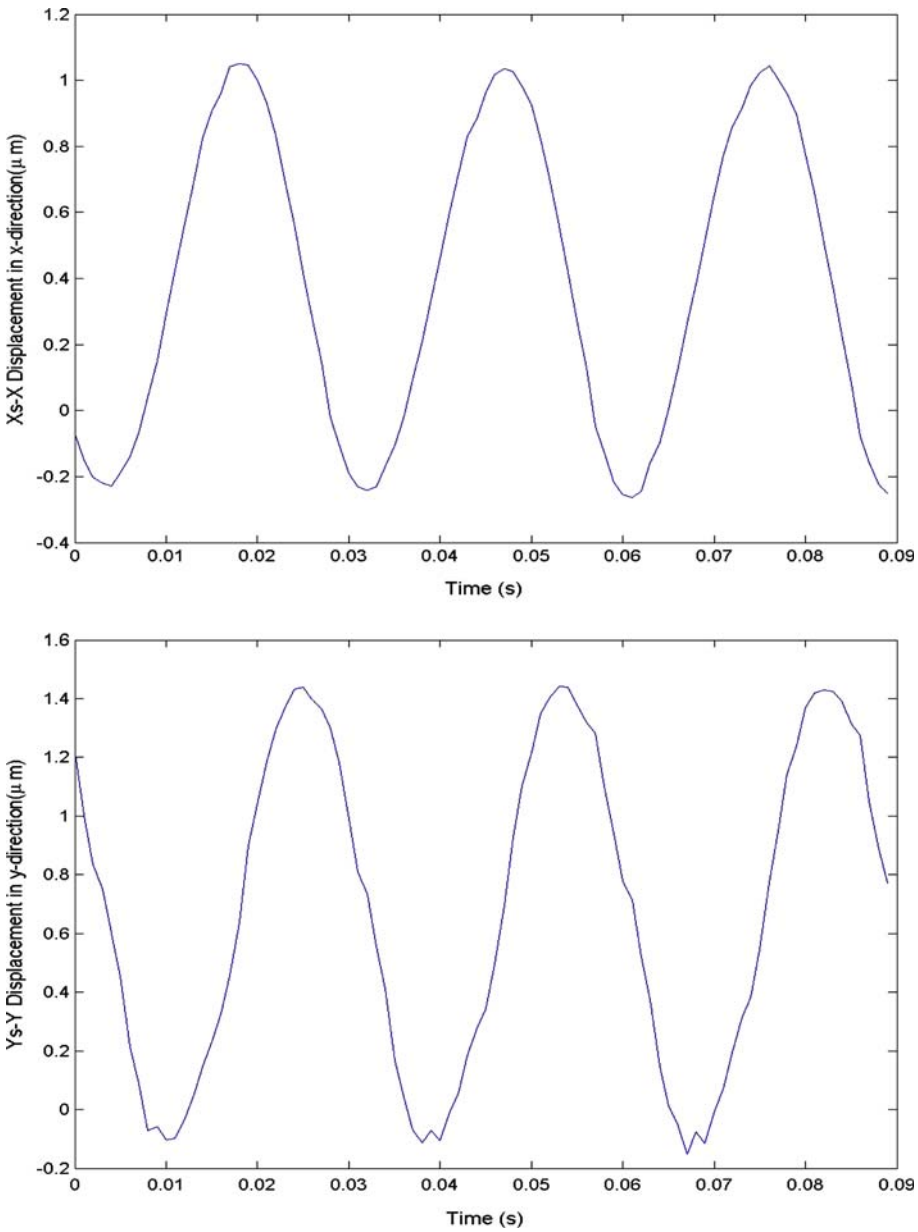

Fig. 10 Measured motion difference between the spindle and bearing

attitude angle found herein also conforms to common understanding on an HJB (Kawabata et al. 1989; Chao and Haung 2005). It is seen from this figure that the theoretical angles for 3,500 rpm are between experimental counterparts of 3,000 and 4,000 rpms, validating again the performance of the built inspection machine. Figures 13 and 14 show, respectively, the bearing stiffnesses of k_{yy} (direct stiffness) and k_{yx} (cross-coupled stiffness) as opposed to rotor eccentricity and for various rotor speeds. The identified k_{xx} and k_{xy} are not shown herein due to their similarity to k_{yy} and k_{yx}, respectively. It is seen from Figs. 13 and 14 that k_{yy} increases almost exponentially as the rotor eccentricity increases, while k_{yx}, as all negative, decreases almost exponentially as the rotor eccentricity increases. It should be noted at this point that as rotor speed increases, k_{yy} decreases slightly, which is due to the magnification in the inertial effects. Also seen in Figs. 13, 14 is the closeness between the previous theoretical predictions documented in the past studies and the identified counterparts presented in this study. The identified stiffnesses at 3,500 rpms are all between those counterparts of 3,000 and 4,000 rpms.

5 Conclusion and future works

An in situ inspection machine has been successfully designed and constructed successfully in the laboratory for

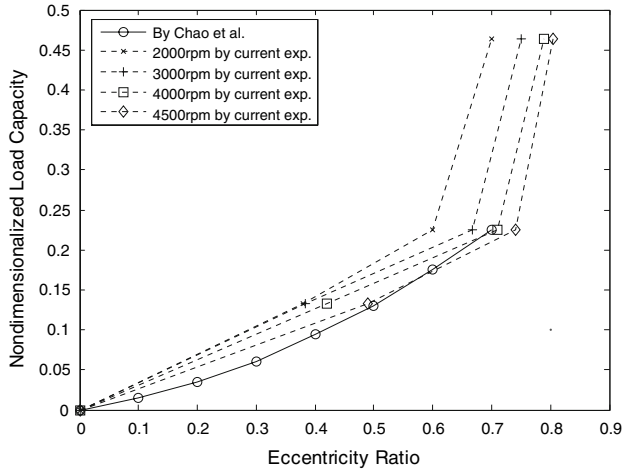

Fig. 11 The load capacity with respect to eccentricity ratio in various rotor speeds

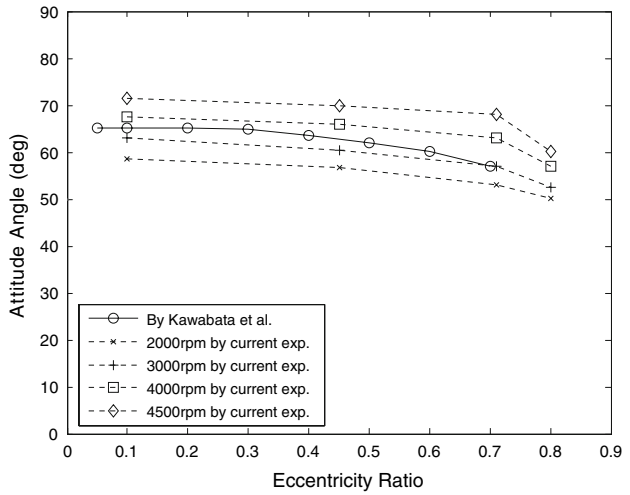

Fig. 12 The attitude angle versus eccentricity ratio

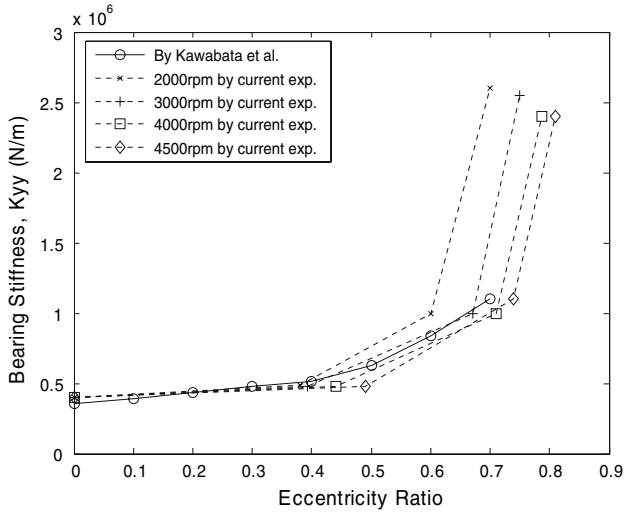

Fig. 13 The bearing stiffnesses k_{yy} versus eccentricity ratio

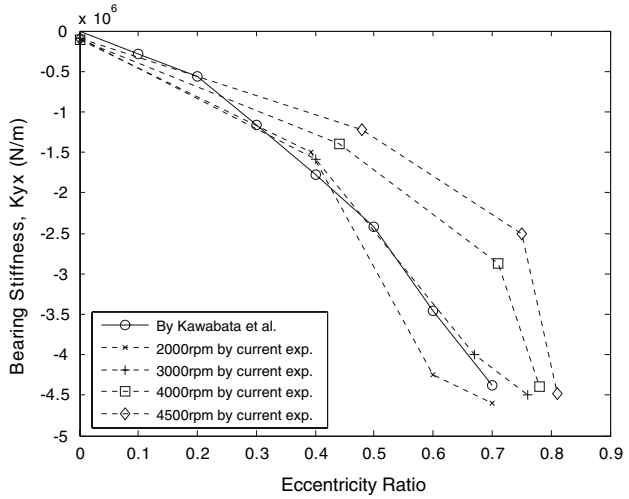

Fig. 14 The bearing stiffnesses k_{yx} versus eccentricity ratio

testing the performance of a small-scaled hydrodynamic journal bearing (HJB) frequently used in data-storage drives, such as hard disc drives and optical disc ones. The key component of the machine is the high stiffness air bearing that keeps the spindle runouts within 1 um. The performance indices of the bearing identified from the experimental data have reflected realistic dynamic characteristics of a small-scaled HJB documented in the past studies, validating the effectiveness of the constructed machine. In the future, in order to improve the S/N ratio of the raw time-domain experimental data, the assembling tightness of the flexible coupling should be re-determined systematically based on theoretical analysis in order to render the spindle runouts as small as possible.

Appendix 1

Technique for reducing data noise

Spectral density averaging techniques are used to obtain the frequency-response functions (FRF) of Eq. (6) for damping out noises, which defines a multi-input multi-output (MIMO) system. The inputs are D_{xx}, D_{xy}, D_{yx}, and D_{yy}, and the outputs are $F_{\mathrm{xx}} - M_s A_{xx}$, $F_{xy} - M_s A_{xy}$, $F_{\mathrm{yx}} - M_s A_{yx}$, and $F_{yy} - M_s A_{yy}$. Before calculating the FRF for this MIMO system, first consider the best solution for the FRF of a single-input single-output (SISO) system. A SISO system with a clean input a and a noise contaminated output b will be examined. According to Bendat and Peirsol (1986), an unbiased estimate H of the FRF for this type of SISO system is given by,

$$H = \frac{G_{ab}}{G_{aa}} \tag{8}$$

with G_{ab} being the cross spectral density and G_{aa} the auto spectral density. For discrete data (which we have) an FFT algorithm is used to calculate the Discrete Fourier Transforms (DFT's) of Eq. (7). In particular, the spectral densities are calculated by,

$$G_{ap} = \frac{2}{n_d N \Delta t} \sum_{i=1}^{n_d} A_i * (\omega) P_i(\omega) \tag{9}$$

where n_d is the number of statistically independent blocks of data, N is the number of data points in each data block, Δt is the time increment between sampling of each data point, $A^*(\omega) =$ the complex conjugate of $\Im\{a(t)\}$ and $P(\omega) = \Im\{p(t)\}$ $\Im$ is used to represent the DFT here).

We wish to apply the unbiased estimator for the SISO system described above to the MIMO system of Eq. (8). First, recall that we have 32 statistically independent blocks of data ($n_d = 32$), each block containing 1,024 ($N = 1{,}024$) data points for each of the dynamic loads, accelerations, and relative motions whose $\Im$ appear in Eq. (8). Next, we identify each independent dynamic load of Eq. (8) (F_{xx} and F_{yy}) as a clean input a, and each of the resulting elements of the force and displacement matrices as noise contaminated outputs b. Eq. (8) is then applied separately to each individual element of the force and displacement matrices, yielding an unbiased estimate for each input and output element contained in these matrices, The resulting equation,

$$\begin{bmatrix} 1 - M_s \frac{G_{fxxaxx}}{G_{fxxfxx}} & \frac{G_{fyyfxy}}{G_{fyyfyy}} - M_s \frac{G_{fyyaxy}}{G_{fyyfyy}} \\ \frac{G_{fxxfyx}}{G_{fxxfxx}} - M_s \frac{G_{fxxayx}}{G_{fxxfxx}} & 1 - M_s \frac{G_{fyyayy}}{G_{fyyfyy}} \end{bmatrix} = \begin{bmatrix} H_{xx} & H_{xy} \\ H_{yy} & H_{yx} \end{bmatrix} \begin{bmatrix} \frac{G_{fxxdxx}}{G_{fxxfxx}} & M_s \frac{G_{fyydxy}}{G_{fyyfyy}} \\ \frac{G_{fxxdyx}}{G_{fxxfxx}} & \frac{G_{fyydyy}}{G_{fyyfyy}} \end{bmatrix}, \tag{10}$$

yields improved estimates for the FRF when solved.

References

Bendat JS, Piersol AG (1986) Deposition of wave forces into linear and nonlinear components. J Sound Vib 106:391–408

Brockwell K, Dmochowski W (1989) Experimental determination of the journal bearing oil film coefficients by the method of selective vibration orbits. 12th biennial conference on mechanical vibration and noise, rotating machinery dynamics, vol 18-1. ASME Publication DE, pp 251–259

Burrows CR, Kucuk NC, Sahinkaya MN, Stanway RS (1987) Estimation of squeeze-film bearing inertia, damping and stiffness coefficients. 11th biennial conference of mechanical vibration and noise, rotating machinery dynamics, vol 2. ASME Publication DE, pp 109–114

Chao PCP, Haung JS (2005) Calculating rotordynamic coefficients of a ferrofluid -lubricated and herringbone-grooved journal bearing via finite difference analysis. Tribol Lett 19(2):101–110. doi: 10.1007/s11249-005-8299-6

Childs D, Hale K (1994) Test apparatus and facility to identify the rotordynamic coefficients of high-speed hydrostatic bearings. ASME J Tribol 116:337–344

Fritzen CP, Seibold S (1990) Identification of mechanical systems by means of the extended kalman filter. Proceedings of the 3rd international conference on rotordynamics, Lyon France, pp 423–429

Kawabata N, Ozawa Y, Kamaya S, Miyake Y (1989) Static characteristics of the regular and reversible rotation type herringbone grooved journal bearing. ASME J Tribol 111:484–490

Mohanmmad ZY, Burdess JS (1990) Identification of journal bearing stiffness and damping coefficients by extended kalman filter. Proceedings of the 3rd international conference on rotordynamics, Lyon France, pp 445–451

Nordmann R, Massmann H (1984) Identification of dynamic coefficients of annular seals. Workshop on rotordynamic instability problems in high performance turbomachinery, Texas A&M University, pp 295–311, NASA CP2338,

Rouvas C, Murphy BT, Hale RK (1992) Bearing parameter identification using power spectral density methods. Submitted to the IMechE fifth international conference on vibrations in rotating machinery

Yasuda C, Kanki H, Ozawa Y, Kawakami T (1986) Application of random excitation technique to dynamic characteristics measurement of bearing. The international conference on rotordynamics, Tokyo, pp 61–67

Zhang QD, Chen SX, Liu ZJ (1999) Design of a hybrid fluid bearing system for HDD spindles. IEEE Trans Magn 35(2):2638–2640. doi:10.1109/20.753792